



OPEN ACCESS

EDITED BY

Divya Lakshmanan,
Yenepoya University, India

REVIEWED BY

Abdul Bari Shah,
Korea University, Republic of Korea
Gini Besant,
Northwestern University, United States
Arathi Prabhaskar,
Indian Institute of Science (IISc), India

*CORRESPONDENCE

Li Rao
✉ raoli0728@163.com
Guo-Ping Yin
✉ yinguoping16@swu.edu.cn

RECEIVED 26 August 2024

ACCEPTED 09 January 2025

PUBLISHED 28 January 2025

CITATION

Xia Y-P, Xie Y, Rao L and Yin G-P (2025)
Bioactive sorbicillinoid derivatives from an
endophytic fungus *Trichoderma citrinoviride*.
Front. Microbiol. 16:1485032.
doi: 10.3389/fmicb.2025.1485032

COPYRIGHT

© 2025 Xia, Xie, Rao and Yin. This is an
open-access article distributed under the
terms of the [Creative Commons Attribution
License \(CC BY\)](#). The use, distribution or
reproduction in other forums is permitted,
provided the original author(s) and the
copyright owner(s) are credited and that the
original publication in this journal is cited, in
accordance with accepted academic
practice. No use, distribution or reproduction
is permitted which does not comply with
these terms.

Bioactive sorbicillinoid derivatives from an endophytic fungus *Trichoderma citrinoviride*

Yan-Ping Xia¹, Yan Xie², Li Rao^{3*} and Guo-Ping Yin^{4*}

¹Department of Pharmacy, Nanan People's Hospital of Chongqing, Chongqing, China, ²Department of Pharmacy, Zhengzhou Shuqing Medical College, Zhengzhou, China, ³Chongqing Key Laboratory of High Active Traditional Chinese Drug Delivery System, Chongqing Medical and Pharmaceutical College, Chongqing, China, ⁴Engineering Research Center of Coptis Development and Utilization (Ministry of Education), College of Pharmaceutical Sciences and Chinese Medicine, Southwest University, Chongqing, China

Three new sorbicillinoid derivatives, citrinsorbicillinol A-C (**1–3**), along with three known compounds, such as trichosorbicillin G (**4**), dibutyl phthalate (**5**), and 3-(4-methoxyphenyl) propanoic acid (**6**), were isolated from the endophyte *Trichoderma citrinoviride* of *Coptis chinensis*. Their structures were elucidated through extensive analyses of spectroscopic data, computer-assisted structure elucidation (ACD/Structure Elucidator), density functional theory (DFT) calculations of the nuclear magnetic resonance (NMR) spectra, and electronic circular dichroism (ECD). Biologically, compounds **1–4** exhibited potential antioxidant activity, as assessed using the 1,1-diphenyl-2-picrylhydrazyl (DPPH) assay, with IC₅₀ values ranging from 27.8 to 89.6 μM. In particular, compounds **2** and **3** demonstrated radical scavenging activity comparable to that of the positive control, ascorbic acid, with IC₅₀ values of 27.8 and 31.2 μM, respectively. Moreover, compound **1** exhibited potential anti-inflammatory activity by inhibiting nitric oxide (NO) production in lipopolysaccharide (LPS)-induced RAW 264.7 macrophages, with an IC₅₀ value of 52.7 μM. These findings underscore the therapeutic potential of the new sorbicillinoid derivatives for antioxidant and anti-inflammatory applications.

KEYWORDS

sorbicillinoid, fungus, *Trichoderma*, antioxidant, anti-inflammatory

1 Introduction

Fungal secondary metabolites are crucial due to their broad chemical diversity and biological activities, making them highly valuable in fields such as medicine (Cai et al., 2024). In particular, fungi from extreme environments, such as endophytes in medicinal plants and marine fungi, often have the ability to produce novel secondary metabolites (Barzkar et al., 2024; Yu et al., 2024). It is essential to thoroughly explore these rare fungi, as this could lead to the discovery of new compounds with unprecedented properties, thereby fully unlocking their potential and advancing our understanding and utilization of fungal secondary metabolites. *Coptis chinensis* Franch., known for its dried rhizomes as a source of the traditional Chinese medicine “Huang lian,” primarily grows in high-altitude areas (1,500–1,800 meters) such as Chongqing, Sichuan, and Hubei provinces in China. Pharmacological studies have shown that its chemical constituents, mainly alkaloids such as berberine, possess significant biological activities, including antibacterial, antitumor, and antidiabetic effects. The high-altitude environment, along with its internal chemical conditions, provides a unique habitat for endophytic fungi, which may produce distinctive secondary metabolites. However, there have been few reports on the secondary metabolites of endophytic fungi in *Coptis chinensis* to date (Zhang et al., 2018; Yin et al., 2021a; Yin et al., 2024).

Sorbicillinoids, a family of metabolites with hexaketide structures, are primarily derived from fungal sources (Xie et al., 2021; Peng et al., 2022). These structures feature a flexible hexacyclic ring and a sorbyl side chain that can undergo reactions such as the Michael addition or the Diels–Alder reaction, resulting in highly oxygenated and polycyclic carbon skeletons (Kahlert et al., 2020; Sib and Gulder, 2017; Rehman et al., 2020). To date, nearly 195 naturally occurring sorbicillinoids have been identified. They are recognized for their diverse biological activities, including anticancer effects, radical scavenging properties, and antibacterial activity (Chen et al., 2022; Wang et al., 2022; Zhao et al., 2022; Wang et al., 2023; Yin et al., 2024; Ying et al., 2024; Zhang et al., 2024a; Zhang et al., 2024b). In our ongoing endeavor to search for structurally unique and biologically interesting metabolites from fungal resources (Yin et al., 2021a; Yin et al., 2024; Wang et al., 2024), the fungus *Trichoderma citrinoviride* was isolated from the rhizomes of a 5-year-old *Coptis chinensis* plant collected from Shizhu, Chongqing. Through solid-state fermentation using rice, six compounds were isolated and identified, including three new sorbicillinoid derivatives, citrinsorbicillinol A–C (1–3), along with three known compounds—trichosorbicillin G (4), dibutyl phthalate (5), and 3-(4-Methoxyphenyl) propanoic acid (6). Herein, the details of their isolation, structural elucidation, and bioactivities are presented.

2 Materials and methods

2.1 General experimental procedures

UV spectra were recorded using a UV-2450 visible spectrophotometer (Shimadzu, Japan). IR spectra (KBr disks) were obtained using a Shimadzu IRPrestige-21 instrument (Shimadzu, Japan). A JASCO J-815 spectropolarimeter was used to measure electronic circular dichroism (ECD) spectra (JASCO, Japan). Nuclear magnetic resonance (NMR) spectra were recorded on a Bruker Advance III 400 spectrometer (Bruker, Germany), with tetramethylsilane (TMS) as the internal standard. High-resolution electrospray ionization mass spectra (HRESIMS) were acquired using a Bruker impact II Q-TOF mass spectrometer (Bruker, Germany) and an Agilent 6520B mass spectrometer (Agilent, American). Analytical high-performance liquid chromatography (HPLC) was conducted with a Shimadzu LC-20 AD pump and a SPD-M20A UV detector (Shimadzu, Japan), using a YMC RP-C18 column (5 μ m, 4.6 \times 250 mm). Preparative high-performance liquid chromatography (HPLC) was performed on a Separation LC-UV system (Separation, China) using a YMC RP-C18 column (5 μ m, 10 \times 250 mm). The flow rate was set at 3.0 ml/min, and detection was carried out at wavelengths of 210 nm and 254 nm using a dual-channel UV detector. Column chromatography was performed using silica gel (100–200 and 200–300 mesh, Qingdao Marine Chemical Inc., China), MCI (50 μ m, Mitsubishi, Japan), and Sephadex LH-20 (Pharmacia Fine Chemical Co., Ltd.).

2.2 Fungal material and identification

The endophytic fungus was obtained from the traditional Chinese medicinal herb *Coptis chinensis* Franch. through the plate coating method, which were collected from Shizhu, Chongqing, China. The isolated strain was identified as *Trichoderma citrinoviride* based on

morphological characteristics, and this identification was further supported by 18S rDNA and internal transcribed spacer (ITS) sequences, which showed 100% identity to the known *Trichoderma citrinoviride* (GenBank Accession KY750459.1). The basic characteristics of *Trichoderma citrinoviride* growth are as follows (Supplementary Figures S29, S30): When *Trichoderma citrinoviride* is inoculated onto a potato dextrose agar (PDA) medium at 28°C, the colony grows rapidly and exhibits aerial mycelium. During the first 1–3 days, the colony appears light green on the surface and yellowish-green on the reverse side, with a transparent mycelium. By the 4th day, extensive areas of white, fluffy colonies begin to appear. By the 5th day, the colonies become a cottony, olive-green mass. The mycelium is septate, and the conidiophores are characterized by a long main axis with shorter secondary branches, which are alternately arranged with unequal spacing and branching at acute or nearly right angles. Some of the terminal branches are flask-shaped, and the phialides bear smooth-walled spores. The conidia are colorless to green, ellipsoidal, and relatively small. The sequence information of this fungus is as follows:

```
GGATCACCTGATCCGAGGTCACATTTTCAGAGTTTGGGGT
GTTTTACGGCTGTGGCCGCGCCGCTCCCGGTGCGAGTG
TGCAAATACTGCGCAGGAGAGGCTGCGGCGAGACCGCC
ACTGTATTTTCGGGGGCGCCCGGTGAGGGGCCGATC CCCA
ACGCCGACCCCCGGAGGGGTTTCGAGGGTTGAAATGACG
CTCGGACAGGCATGCCCCGCAATACTGGCGGGGCGC AAT
GTGCGTTCAAAGATTTCGATGATTCACCTGAATTCGCAATTC
ACATTACTTATCGCATTTTCGCTGCGTTCTTCATCGATGCCA
GAACCAAGAGATCCGTTGTTGAAAGTTTTGATTCATTTTCG
AGACGCCCCGCTAGGGTTCGCCGAGAAAGGCTCAGAGCAAAA
ATAAAACAGAGCCGCGACGTAGGCCGCGACGGAGAGAAAA
AAGAGTTTGAGTTGGTCCTCCGGCGGGCGCCATGGGATCC
GGGGCTGCGACGCGCCCCGGGGCAGAGAATCCCGCCGA GGC
AACAGATTGGTAACGTTTCACATTTGGGTTTGGGAGTTGTAA
ACTCGGTAATGATCCCTCCGCTGGTTACCAACGGAGACCT
TGTT CCCTT.
```

2.3 Fermentation and extraction

The strain was cultured on potato dextrose agar (PDA) at 28°C for 7 days. Then, two pieces of the agar (about 1.0 cm³) were added to an Erlenmeyer flask (250 ml) containing 100 ml of potato dextrose liquid medium. The flask was then incubated on a rotary shaker at 28°C and 150 rpm for 5 days to prepare the seed culture. Solid fermentation was carried out in 400 Erlenmeyer flasks (1 L each). The flasks were sterilized by autoclaving prior to use and contained 200 g of rice, 1.0 g of glucose, 0.5 g of CuSO₄•5H₂O, and 200 ml of distilled water. All flasks were incubated at room temperature for 30 days. The solid cultures were extracted with ethyl acetate (EtOAc) three times at room temperature. The solvent was removed under reduced pressure to yield 1,000 g of crude extract.

2.4 Isolation of the metabolites

The crude extract (1,000 g) was subjected to silica gel column chromatography (CC), and elution was performed using a mixture of petroleum ether (boiling point, 60–90°C) and EtOAc in ratios ranging from 15:1 to 0:1, resulting in increasing polarity. This process

yielded eight fractions (Fr.1–8), as determined by thin layer chromatography (TLC) analysis. Fr. 5 (150 g) was further fractionated by repeated CC on silica gel, again eluting with petroleum ether and EtOAc (15:1 to 0:1), to produce seven subfractions (Fr.5.1–5.7). Fr.5.3 (45 g) was subjected to additional silica gel CC, eluting with the same solvent system to generate five fractions (Fr.5.3.1–5.3.5). Fr.5.3.2 (9.7 g) was then separated using MCI CC with gradient elution (MeOH/H₂O, 30:70 to 100:0), resulting in 154 subfractions (Fr.5.3.2.1–5.3.2.154). Specific subfractions were purified by semi-preparative HPLC as follows: Fr.5.3.2.12 (37.8 mg) was purified using ACN/H₂O (38:62, 3 ml/min) to obtain compound **3** (12.1 mg, $t_R = 19.3$ min; proportion of total extract, 0.00121%). Fr.5.3.2.26 (25.6 mg) yielded compound **2** (12.3 mg, $t_R = 55.2$ min; proportion of total extract, 0.00123%) after purification with MeOH/H₂O (63:37, 3 ml/min). Compound **6** (9.0 mg, $t_R = 19.9$ min; proportion of total extract, 0.0009%) was purified from Fr.5.3.2.28 (17.5 mg) using MeOH/H₂O (43:57, 3 ml/min). Fr.5.3.2.48 (25.7 mg) resulted in compound **5** (11.9 mg, $t_R = 22.2$ min; proportion of total extract, 0.00119%) after purification with ACN/H₂O (80:20, 3 ml/min). Separately, Fr.5.4 (7.6 g) was fractionated using Sephadex LH-20 with CH₂Cl₂-MeOH (1:1) to produce four subfractions (Fr.5.4.1–5.4.4). Fr.5.4.3 (3.1 g) was further separated by MCI CC through gradient elution with MeOH/H₂O (30:70 to 100:0) to yield 21 subfractions (Fr.5.4.3.1–5.4.3.21). Compound **1** (15.3 mg, $t_R = 67.4$ min; proportion of total extract, 0.00153%) was purified from Fr.5.4.3.12 (35.2 mg) using MeOH/H₂O (40:60, 3 ml/min). Finally, compound **4** (9.1 mg, $t_R = 39.1$ min; proportion of total extract, 0.00091%) was obtained from Fr.5.4.3.15 (31.2 mg) after purification with MeOH/H₂O (50:50, 3 ml/min).

Citrinsorbicillinol A (**1**): yellow powder; UV (MeOH) (log ϵ) λ_{max} 229 (3.06), 261 (3.61), 282 (2.85), 366 (3.38) nm; IR (KBr) ν_{max}/cm^{-1}

3,752, 3,689, 2,372, 1701, 1,655, 1,544, 1,386, 1,155, 1,107, 1,026; HRESIMS m/z 237.0799 [M + H]⁺ (calcd for C₁₂H₁₃O₅⁺ 237.0763); ¹H NMR and ¹³C NMR data, see Table 1.

Citrinsorbicillinol B (**2**): yellow oil; [α]₂₅ D -26.5 (*c* 0.24, ACN); ECD (ACN) λ_{max} ($\Delta\epsilon$) 218 (-4.17), 297 (+1.55), 344 (-1.95) nm; UV (MeOH) (log ϵ) λ_{max} 216 (3.63), 249 (2.81), 286 (3.55), 331 (2.96) nm; IR (KBr) ν_{max}/cm^{-1} 3,751, 3,689, 3,651, 2,931, 2,376, 1739, 1718, 1,621, 1,560, 1,523, 1,388, 1,305, 1,232, 1,161, 1,111, 1,022; HRESIMS m/z 301.1415 [M + Na]⁺ (calcd for C₁₆H₂₂O₄Na⁺ 301.1416); ¹H NMR and ¹³C NMR data, see Table 1.

Citrinsorbicillinol C (**3**): yellow powder; [α]₂₅ D -20.4 (*c* 0.22, ACN); ECD (ACN) λ_{max} ($\Delta\epsilon$) 217 (-2.54), 284 (+1.70), 324 (-1.11) nm; UV (MeOH) (log ϵ) λ_{max} 217 (3.45), 249 (2.36), 385 (3.36), 330 (2.98) nm; IR (KBr) ν_{max}/cm^{-1} 3,398, 2,927, 2,378, 1712, 1,678, 1,662, 1,625, 1,537, 1,519, 1,487, 1,452, 1,384, 1,230, 1,166, 1,026; HRESIMS m/z 247.0946 [M + Na]⁺ (calcd for C₁₂H₁₆O₄Na⁺ 247.0955); ¹H NMR and ¹³C NMR data, see Table 1.

2.5 Conformational optimization

The initial conformational analysis of compounds **1–3** was carried out using the SPARTAN¹⁴ program, which employed the Monte Carlo searching algorithm with the MMFF94 molecular mechanics force field (Halgren, 1999). This resulted in a set of relatively stable conformations within an energy range of 3 kcal/mol above the global minimum. The conformers with minimum energy from the force field were then further optimized using density functional theory (DFT) at the B3LYP/6-31G(d) level, as implemented in the Gaussian 16 program. To ensure the reliability of the optimized conformers, harmonic vibrational frequency calculations were performed,

TABLE 1 ¹H NMR (400 MHz) and ¹³C NMR (100 MHz) spectroscopic data for compounds **1–3**.

Position	1 (DMSO- <i>d</i> ₆)		Position	2 (CDCl ₃)		3 (CDCl ₃)	
	δ_H (J in Hz)	δ_C		δ_H (J in Hz)	δ_C	δ_H (J in Hz)	δ_C
1		163.6	1		113.3		113.2
2		102.8	2	7.36 (s)	129.2	7.36 (s)	129.1
3		165.9	3		114.9		114.9
4	6.80 (s)	99.5	4		159.2		159.2
5		156.0	5		110.5		110.5
6	6.72 (d, 15.0)	129.6	6-OH	12.73 (s)	161.6	12.70 (s)	161.6
7	7.11 (dd, 15.0, 11.4)	131.9	7		204.4		204.3
8	7.25 (dd, 15.0, 11.4)	141.5	8	3.06 (m)	44.3	3.00 (dd, 17.2, 8.7) 3.11 (dd, 17.2, 3.0)	45.7
9	6.25 (d, 15.0)	128.2	9	4.21 (m)	67.4	4.40 (dq, 8.7, 6.3, 3.0)	64.3
10		168.0	10	1.58 (m)	36.4	1.31 (d, 6.3)	22.5
2-Me	1.83 (s)	9.4	11	2.16 (overlap)	28.7		
3-OMe	3.92 (s)	57.3	12	5.45 (overlap)	130.6		
			13	5.50 (overlap)	125.6		
			14	1.66 (d, 4.9)	17.9		
			3-Me	2.21 (s)	15.6	2.21 (s)	15.6
			5-Me	2.13 (s)	7.4	2.13 (s)	7.4

confirming the absence of imaginary frequencies. The conformers accounting for over 99% of the population were then subjected to subsequent calculations.

2.6 ECD calculations

The predominant conformers of compounds **2** and **3** were subjected to theoretical ECD calculations using time-dependent density functional theory (TDDFT) at the M062X/def2SVP level in acetonitrile, employing the conductor-like polarizable continuum model (CPCM) for the solvent model. For each conformer, 30 excited states were calculated. The energies, oscillator strengths, and rotational strengths of each conformer were computed using the Gaussian 16 program. The ECD spectra for each conformer were approximated using Gaussian distributions. Finally, the overall ECD spectrum was determined by summing the spectra of individual conformers, weighted according to their Boltzmann populations, using the SpecDis v1.71 program (Bruhn et al., 2013).

2.7 ¹³C NMR calculations

The NMR shielding constants were calculated using the gauge-independent atomic orbital (GIAO) method at the mPW1PW91-SCRF/6-31 + G(2d,p) level with the PCM solvent model in dimethyl sulfoxide (DMSO). The shielding constants obtained were converted into chemical shifts by referencing TMS at 0 ppm ($\delta_{\text{cal}} = \sigma_{\text{TMS}} - \sigma_{\text{cal}}$), where σ_{TMS} was the shielding constant of TMS calculated at the same level (Willoughby et al., 2014). The DP4+ probabilities for each possible candidate were calculated using the Excel spreadsheet provided by Grimblat et al. (2015). For each possible candidate, we calculated the parameters a and b of the linear regression $\delta_{\text{cal}} = a\delta_{\text{exp}} + b$. Additionally, we computed the correlation coefficient, R^2 , the mean absolute error (MAE), which is defined as $\sum n|\delta_{\text{cal}} - \delta_{\text{exp}}|/n$, and the corrected mean absolute error (CMAE), which is defined as $\sum n|\delta_{\text{corr}} - \delta_{\text{exp}}|/n$, where $\delta_{\text{corr}} = (\delta_{\text{cal}} - b)/a$.

2.8 DPPH radical-scavenging activity

The antioxidant activity of compounds **1–6** was assessed based on their scavenging activity against the stable 1,1-diphenyl-2-picrylhydrazyl (DPPH) radical (Zhao et al., 2010).

Samples in methanol, with concentrations ranging from 2 to 200 $\mu\text{g/ml}$, were mixed with freshly prepared 0.1 mM DPPH in ethanol. Absorbance at 517 nm was measured after 30 min at room temperature. Anhydrous ethanol served as the blank control, and ascorbic acid was used as the positive control. The radical-scavenging activity was expressed as the percentage inhibition, calculated using the following formula: Inhibition (%) = $[A_{\text{control}} - (A_{\text{sample}} - A_{\text{blank}})]/A_{\text{control}} \times 100\%$. Three parallel experiments were performed.

2.9 Measurement of NO production

The inhibition of lipopolysaccharide-induced nitric oxide (NO) production in RAW 264.7 mouse macrophage cells was evaluated as follows (Kumar et al., 2024; Yin et al., 2021b): The cells were evaluated

using 96-well plates (1×10^5 cells/well) and allowed to adhere for 2 h at 37°C in 5% CO₂ in air. Then, the cells were treated with 1 $\mu\text{g/ml}$ lipopolysaccharide (LPS) for 24 h, with or without the test compound (5 $\mu\text{g/ml}$). DMSO was used as the solvent. All compounds were tested at a final concentration of 0.2% (v/v) in the cell-culture supernatant. The NO production was determined by measuring the accumulation of nitrite in the culture supernatant using the Griess reagent. The absorbance of the mixture was read at 540 nm using a microplate reader. L-NAME (*N*^o-nitro-L-arginine methyl ester) was used as the positive control. Data were presented based on three parallel experiments.

2.10 Data and statistical analysis

The data were expressed as mean \pm SD. Error bars represented the three independent experiments. p -values were calculated using ordinary one-way ANOVA.

3 Results and discussion

3.1 Structural elucidation

Citrinsorbicillinol A (**1**) was isolated as a yellow amorphous powder with a purity of over 95%, as determined by the HPLC analysis (Supplementary Figure S26). The molecule formula C₁₂H₁₂O₅ was established by HRESIMS (Supplementary Figure S5) at m/z 237.0799 $[M + H]^+$ (calcd. for C₁₂H₁₃O₅, 237.0763), corresponding to seven degrees of unsaturation. The ¹H NMR data (Supplementary Figure S1 and Table 1) clearly exhibited the presence of 11 protons, including 2 singlet methyl groups at δ_{H} 1.83 and 3.92, a conjugated diene moiety with 4 olefinic protons at δ_{H} 6.25 (d, $J = 15.0$ Hz), 6.72 (d, $J = 15.0$ Hz), 7.11 (dd, $J = 15.0, 11.4$ Hz), and 7.25 (dd, $J = 15.0, 11.4$ Hz), and a singlet aromatic proton at δ_{H} 6.80. The ¹³C NMR data (Supplementary Figure S2 and Table 1) revealed a total of 12 resonances. These resonances were assigned with the help of HSQC data (Supplementary Figure S3) to two methyl groups at δ_{C} 9.4 and 57.3, five sp² methine groups at δ_{C} 99.5, 128.2, 129.6, 131.9, and 141.5, and five non-protonated carbons at 102.8, 156.0, 163.6, 165.9, and 168.0.

The structure of compound **1** was further elucidated through a comprehensive analysis of the 2D NMR data (Figure 1A). The key HMBC correlations (Supplementary Figure S4) from H-9 to C-10 and C-7; from H-8 to C-6, C-7, C-9, and C-10; and from H-6 to C-7 and C-8, along with the coupling constant of the related protons, support the construction of an (*E*)-penta-2,4-dienoic acid moiety. Moreover, the HMBC correlations from H₃-2-Me to C-1, C-2, and C-3; from H₃-3-OMe to C-3; from H-4 to C-2, C-3, C-5, and C-6; and from H-6 to C-4 and C-5, along with the chemical shift of C-5 at δ_{C} 156.0, suggested that the (*E*)-3-methoxy-2-methylpenta-2,4-dienoic acid moiety was connected to the (*E*)-penta-2,4-dienoic acid moiety via the oxygenated olefinic carbon at C-5. Considering the remaining unsaturation and the chemical shifts of C-1 at δ_{C} 163.6 and C-5 at δ_{C} 156.0, a lactone between C-1 and C-5 was deduced to establish the unsaturated six-membered lactone ring (Figure 1A).

To further verify the structure, the computer-assisted structure elucidation (CASE) algorithm was employed. Specifically, ACD/Structure Elucidator (ACD/SE), an advanced CASE expert system,

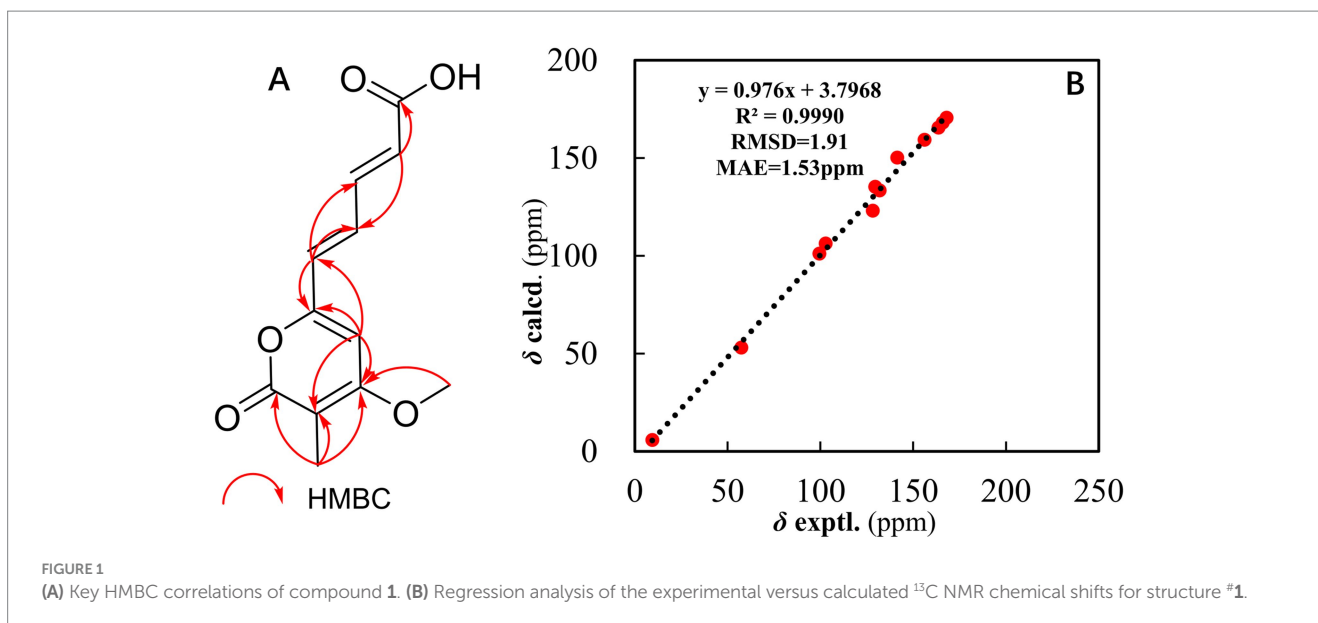


FIGURE 1 (A) Key HMBC correlations of compound 1. (B) Regression analysis of the experimental versus calculated ^{13}C NMR chemical shifts for structure #1.

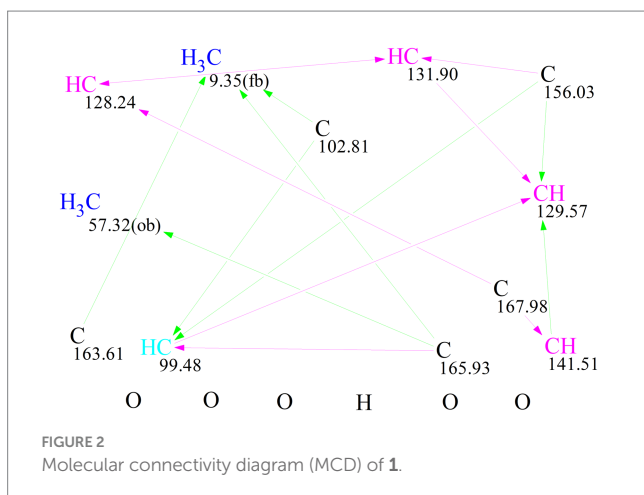


FIGURE 2 Molecular connectivity diagram (MCD) of 1.

was utilized to automatically and efficiently determine the most probable structure based on chemical rules and common knowledge. In recent years, CASE analysis has increasingly been applied to structural revisions and identifications (Fan et al., 2022; Chen et al., 2024). The molecular formula and NMR data of compound 1, which were analyzed using ACD/SE, led to the automatic generation of a molecular connectivity diagram (MCD), as shown in Figure 2. In the MCD (Figure 2), atom hybridization states are color-coded: sp^3 is represented in blue, sp^2 in violet, and undefined hybridization in black. The connecting lines are also color-coded to indicate different types of connectivity: green lines represent HMBC connectivity, and violet lines indicate non-standard connectivity for $^nJ_{\text{HH}}$ and $^nJ_{\text{CH}}$ ($n > 3$).

For each candidate structure, ^1H and ^{13}C chemical shifts were predicted using three empirical methods provided by ACD/SE: HOSE (d_A), the incremental approach (d_I), and neural networks (d_N). The structures that did not meet the threshold criteria of an average C deviation greater than 4 ppm or a maximum C deviation exceeding 20 ppm were discarded. The remaining structures were ranked based

on the average deviation (d_A) of the ^{13}C chemical shifts between experimental and calculated values. The accuracy of the ^{13}C chemical shift predictions was indicated by color-coded circles: green for the deviations ≤ 3 ppm and yellow for the deviations between 3 and 15 ppm. Ultimately, seven candidate structures were generated using ACD/SE from a total of 41,537 structures, and after removing the duplicates, six distinct structures remained, as shown in Figure 3. Among these, structure #1, listed at the top of the output file from the ACD-Lab, exhibited the highest match factor (MF) value ($d_A = 1.605$, $d_N = 1.824$, and $d_I = 1.697$), which further confirmed its structure.

Furthermore, the ^{13}C NMR calculation (Figure 1B) provided strong evidence for the assignment of structure #1. This analysis was performed within the GIAO framework at the MPW1PW91/6-311+G (2d, p) level, and geometries were optimized at the B3LYP/6-31G (d) level in chloroform. The correlation coefficient (R^2) obtained from linear regression analysis between the calculated and experimental ^{13}C NMR data for structure #1 was 0.9990, and the mean absolute error (MAE) was 1.53 ppm. Thus, the structure of compound 1 was constructed (Figure 4).

Citrinsorbicillinol B (2) was obtained as a yellow oil with a purity of over 95%, as determined by the HPLC analysis (Supplementary Figure S27). The molecular formula was determined as $\text{C}_{16}\text{H}_{22}\text{O}_4$ based on a positive HRESIMS (Supplementary Figure S13) peak at m/z 301.1415 [$\text{M} + \text{Na}$] $^+$ (calcd. for $\text{C}_{16}\text{H}_{22}\text{O}_4\text{Na}$, 301.1416), which required six degrees of unsaturation. The ^1H NMR data (Supplementary Figure S8 and Table 1) for compound 2 showed signals for two singlet methyl groups at δ_{H} 2.13 and 2.21, one doublet methyl group at δ_{H} 1.66 (d, $J = 4.9$ Hz), two olefinic protons at δ_{H} 5.50 and 5.45, one aromatic proton at δ_{H} 7.36 (s), and one typical hydroxyl proton at δ_{H} 12.73 (s). The ^{13}C NMR and HSQC data (Supplementary Figures S9, S10 and Table 1) displayed 16 carbon resonances, accounting for three methyl groups at δ_{C} 7.4, 15.6, and 17.9, three sp^3 methylene groups at δ_{C} 28.7, 36.4, and 44.3, three sp^2 methine groups at δ_{C} 125.6, 129.2, and 130.6, one sp^3 methine group at δ_{C} 67.4, and six non-protonated carbons at δ_{C} 110.5, 113.3, 114.9, 159.2, 161.6, and 204.4. In the 2D NMR spectra (Figure 5), the ^1H - ^1H COSY correlations (Supplementary Figure S12) of

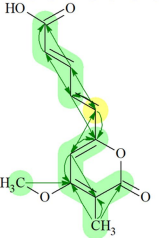
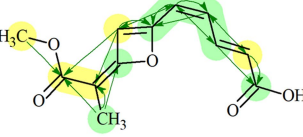
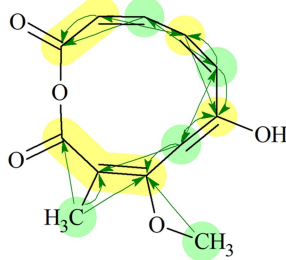
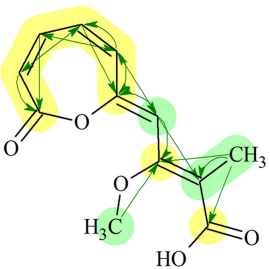
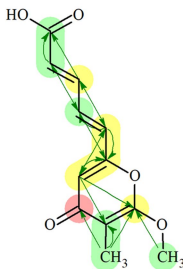
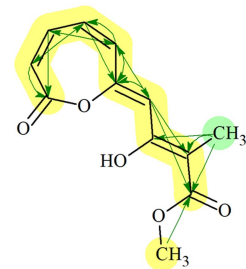
<p>1 (ID:8) The Best Structure</p> 	<p>2 (ID:1)</p> 	<p>3 (ID:10)</p> 
<p>Formula: C₁₂H₁₂O₅ d_T(¹³C): 1.697 d_N(¹³C+¹H): 5.904 d_A(¹³C): 1.605 (v.14.50) d_N(¹³C): 1.824</p>	<p>Formula: C₁₂H₁₂O₅ d_T(¹³C): 4.376 d_N(¹³C+¹H): 6.056 d_A(¹³C): 3.265 (v.14.50) d_N(¹³C): 4.047</p>	<p>Formula: C₁₂H₁₂O₅ d_T(¹³C): 3.438 d_N(¹³C+¹H): 10.260 d_A(¹³C): 4.414 (v.14.50) d_N(¹³C): 5.052</p>
<p>4 (ID:13)</p> 	<p>5 (ID:5)</p> 	<p>6 (ID:4)</p> 
<p>Formula: C₁₂H₁₂O₅ d_T(¹³C): 4.213 d_N(¹³C+¹H): 6.063 d_A(¹³C): 4.513 (v.14.50) d_N(¹³C): 3.993</p>	<p>Formula: C₁₂H₁₂O₅ d_T(¹³C): 3.955 d_N(¹³C+¹H): 8.820 d_A(¹³C): 4.820 (v.14.50) d_N(¹³C): 4.368</p>	<p>Formula: C₁₂H₁₂O₅ d_T(¹³C): 4.140 d_N(¹³C+¹H): 7.412 d_A(¹³C): 5.734 (v.14.50) d_N(¹³C): 4.929</p>

FIGURE 3
The generated six structures in the output file of ACD/SE.

H₃-14/H-13/H-12/H₂-11/H₂-10/H-9/H₂-8, along with the key HMBC correlations (Supplementary Figure S11) from H₃-14 to C-12 and C-13; from H₂-10 to C-11, C-12, C-8, and C-9; and from H₂-8 to C-7, C-9, and C-10, supported the construction of an (*E*)-3-hydroxynon-6-en-1-one moiety. Then, a 2,4-dimethylbenzene-1,3-diol moiety was confirmed by the key HMBC correlations from H₃-3-Me to C-2, C-3, and C-4; from H₃-5-Me to C-4, C-5, and C-6; from H-2 to C-1 and C-6; and from OH-6 to C-1, C-5, and C-6. Moreover, the key HMBC correlations from H-2 to C-7 indicated that the (*E*)-3-hydroxynon-6-en-1-one moiety at C-7 was connected to the 2,4-dimethylbenzene-1,3-diol moiety at C-1 by a C-C single bond. Hence, the planar structure of compound 2 was established (Figure 4).

The absolute configuration of compound 2 was determined using TDDFT calculations of the ECD spectrum with the Gaussian 16 program. The ECD spectrum calculated for the 9*R* configuration was consistent with the experimental ECD spectrum (Figure 6). Hence, the absolute configuration of compound 2 was assigned as 9*R* (Figure 4).

Citrinsorbicillinol C (3) was obtained as a yellow powder with a purity of over 95%, as determined by the HPLC analysis (Supplementary Figure S28). The molecular formula of compound 3 was established as C₁₂H₁₆O₄ based on its HREIMS data (Supplementary Figure S21), indicating that it was the unit of C₄H₆ less than compound 2. Detailed analysis of its NMR spectroscopic (Supplementary Figures S17, S18 and Figure 4) features implied that its chemical structure was very similar to that of compound 2. The main difference was that compound 3 was missing two aliphatic methylene groups and two olefinic methine groups compared to compound 2. Further analysis of the 2D NMR data (Supplementary Figures S19, S20 and Figure 5) showed that the side chain of compound 3 lacked an *n*-butene unit compared to that of compound 2. This was supported by the key HMBC correlations from H₃-3-Me to C-2, C-3, and C-4; from H₃-5-Me to C-4, C-5, and C-6; from H₃-10 to C-8 and C-9; from H₂-8 to C-1 and C-7; from H-2 to C-1 and C-7; and from OH-6 to C-1, C-5, and C-6. Finally, the absolute configuration was established as 9*R* by comparing the experimental ECD spectrum with the calculated one (Figure 7).

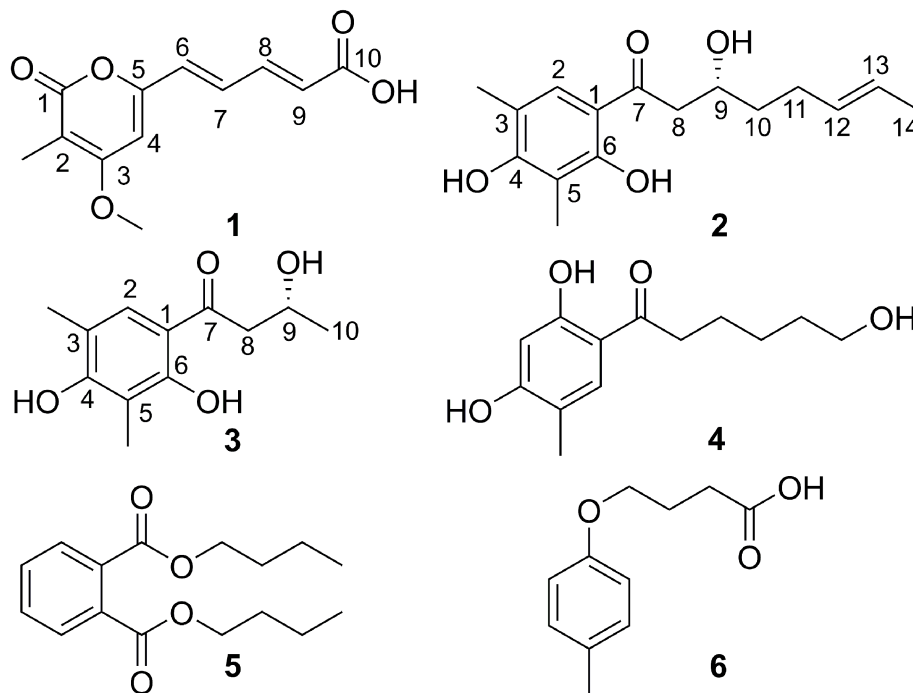


FIGURE 4
Structures of compounds 1–6.

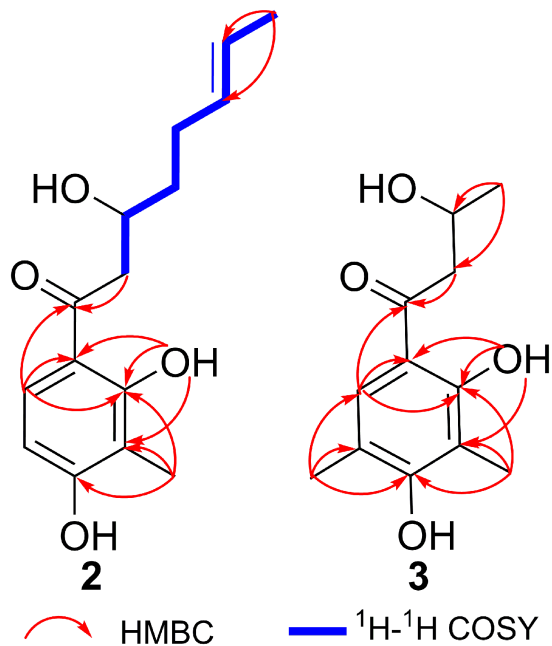


FIGURE 5
Key HMBC correlations of compounds 2 and 3.

In addition, three known compounds were finally characterized as trichosorbicillin G (4) (Zhang et al., 2019), dibutyl phthalate (5) (Li et al., 2009), and 3-(4-Methoxyphenyl) propanoic acid (6) (Zou et al., 2021), by comparing their spectroscopic data with the literature.

3.2 Biological activities

The isolated compounds 1–6 were tested for their antioxidant properties using the DPPH assay (Table 2). As a result, compounds 1–4 exhibited radical scavenging activity, with IC_{50} values ranging from 27.8 to 89.6 μ M. Notably, compounds 2 and 3, with IC_{50} values of 27.8 and 31.2 μ M, respectively, exhibited significant activity comparable to that of ascorbic acid ($IC_{50} = 39.4 \mu$ M). Structurally, compounds 2 and 3 each possessed two identical phenolic hydroxyl groups and one similar alcohol hydroxyl group. Compound 4 had a similar structure but with different substituents on the benzene ring and a different alcohol hydroxyl group. In contrast, compound 1 contained a carboxylic acid group with a long conjugated system. These results indicated that the number and position of phenolic and alcohol hydroxyl groups are crucial for antioxidant activity, with the substituents on the benzene ring also playing a significant role. Furthermore, the presence of a long conjugated carboxylic acid group could be a potent fragment contributing to antioxidant activity.

In addition, all compounds were tested for their inhibitory activities toward nitric oxide (NO) production in lipopolysaccharide (LPS)-induced RAW 264.7 macrophages (Table 2). None of the compounds showed significant cytotoxicity at the concentrations of 50 μ M for the inhibition of the NO production. Among them, only compound 1 showed moderate inhibitory activity, with an IC_{50} value of 52.7 μ M.

4 Conclusion

In this study, three new polyketides 1–3 and three known compounds 4–6 were isolated and identified from the endophytic

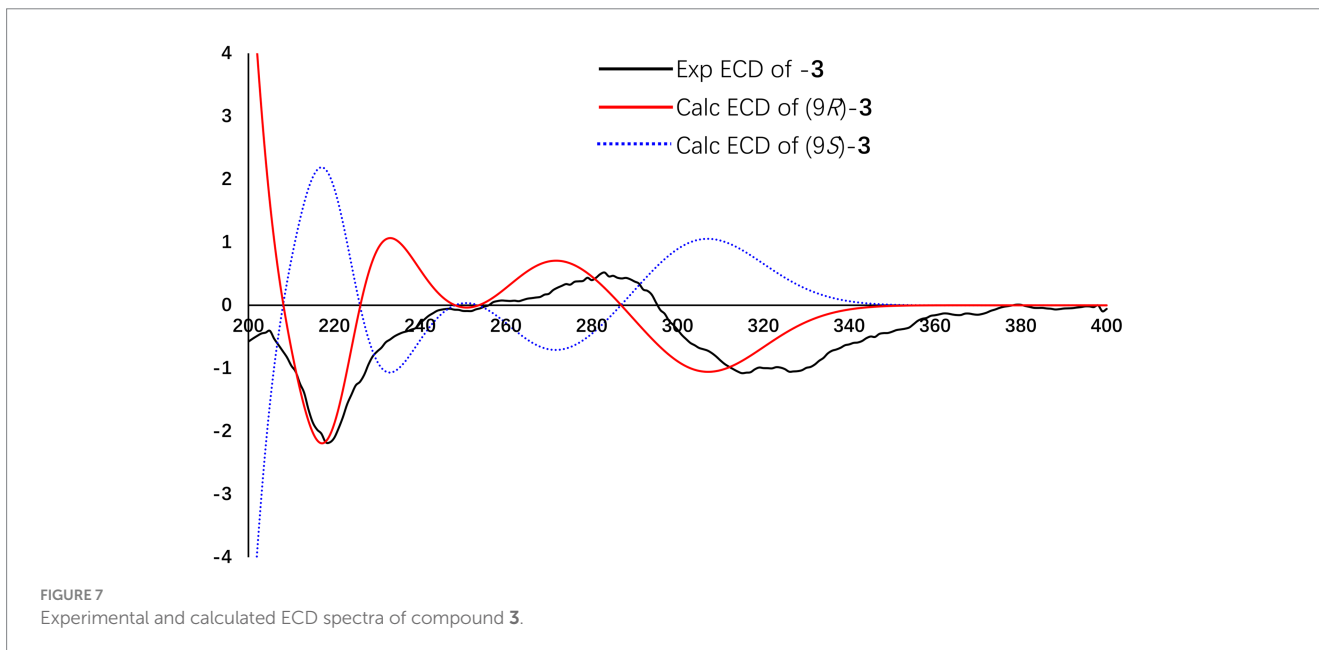
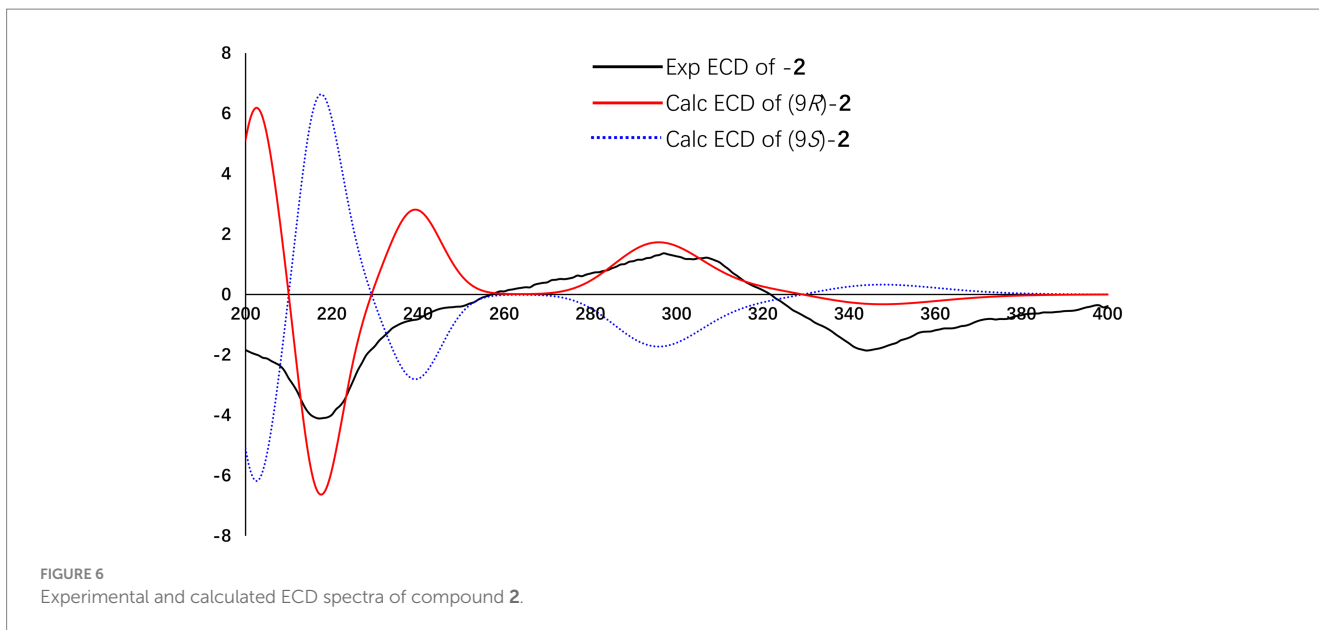


TABLE 2 The DPPH radical-scavenging activity and inhibitory effects on the NO Production of compounds 1–6.

Compounds	IC ₅₀ (μM)	
	DPPH	NO
1	89.6 ± 1.1	52.7 ± 0.8
2	27.8 ± 0.5	>100
3	31.2 ± 0.4	>100
4	51.2 ± 1.0	>100
5	> 100	>100
6	> 100	>100
Ascorbic acid	39.4 ± 0.9	-
L-NAME ^a	-	48.6 ± 0.6

^a *p* < 0.05, compared to the control group.

fungus *Trichoderma citrinoviride* associated with *Coptis chinensis*. The biological assays demonstrated that compounds 1–4 exhibited notable antioxidant activity, highlighting their potential as effective agents in mitigating oxidative damage. Particularly, compounds 2 and 3 showed significant radical scavenging capabilities, comparable to the positive control, ascorbic acid. In addition, compound 1 exhibited promising anti-inflammatory effects by inhibiting the nitric oxide production. Overall, these identified compounds not only contribute to the expanding collection of bioactive natural products but also offer promising avenues for the development of new antioxidant and anti-inflammatory agents. Future work should focus on further exploring the mechanisms underlying these biological activities and assessing the efficacy of these compounds in more complex biological systems.

Data availability statement

The original contributions presented in the study are included in the article/[Supplementary material](#), further inquiries can be directed to the corresponding authors.

Author contributions

Y-PX: Conceptualization, Data curation, Formal analysis, Investigation, Methodology, Software, Writing – original draft, Writing – review & editing. YX: Data curation, Formal analysis, Methodology, Writing – original draft, Writing – review & editing. LR: Data curation, Project administration, Resources, Software, Writing – review & editing. G-PY: Conceptualization, Data curation, Funding acquisition, Investigation, Project administration, Software, Supervision, Writing – review & editing.

Funding

The author(s) declare that financial support was received for the research, authorship, and/or publication of this article. This work was supported by the Open Project of the State Key Laboratory of Natural Medicines (No. SKLNMKF202304), the Fundamental Research Funds for the Central Universities (SWU-KT24002), the National Natural

Science Foundation of China (No. 82003629), and the Natural Science Foundation of Chongqing (No. cstc2021jcyj-msxmX0975).

Conflict of interest

The authors declare that the research was conducted in the absence of any commercial or financial relationships that could be construed as a potential conflict of interest.

Publisher's note

All claims expressed in this article are solely those of the authors and do not necessarily represent those of their affiliated organizations, or those of the publisher, the editors and the reviewers. Any product that may be evaluated in this article, or claim that may be made by its manufacturer, is not guaranteed or endorsed by the publisher.

Supplementary material

The Supplementary material for this article can be found online at: <https://www.frontiersin.org/articles/10.3389/fmicb.2025.1485032/full#supplementary-material>

References

- Barzkar, N., Sukhikh, S., and Babich, O. (2024). Study of marine microorganism metabolites: new resources for bioactive natural products. *Front. Microbiol.* 14:1285902. doi: 10.3389/fmicb.2023.1285902
- Bruhn, T., Schaumlöffel, A., Hemberger, Y., and Bringmann, G. (2013). SpecDis: quantifying the comparison of calculated and experimental electronic circular dichroism spectra. *Chirality* 25, 243–249. doi: 10.1002/chir.22138
- Cai, J., Zhou, X., Wang, B., Zhang, X., Luo, M., Huang, L., et al. (2024). Bioactive polyketides and meroterpenoids from the mangrove-derived fungus *Talaromyces flavus* TGGP35. *Front. Microbiol.* 15:1342843. doi: 10.3389/fmicb.2024.1342843
- Chen, S., Guo, H., Wu, Z., Wu, Q., Jiang, M., Li, H., et al. (2022). Targeted discovery of sorbicillinoid pigments with anti-inflammatory activity from the sponge-derived fungus *Stagonospora* sp. SYSU-MS7888 using the PMG strategy. *J. Agric. Food Chem.* 70, 15116–15125. doi: 10.1021/acs.jafc.2c05940
- Chen, D., Xu, X., Yang, Y., Meng, H., Xu, M., Dong, L., et al. (2024). Discovery of cadinane-type sesquiterpenoids from the infected stems of *Hibiscus tiliaceus* as potential agrochemical fungicides. *J. Agric. Food Chem.* 72, 4089–4099. doi: 10.1021/acs.jafc.3c08508
- Fan, K., Zhang, L. C., Hu, W. Y., Deng, S. Y., Wu, H., Tan, B. Y., et al. (2022). Tabernaecorymine a, an 18-normoterpenoid indole alkaloid with antibacterial activity from *Tabernaemontana corymbosa*. *Fitoterapia* 157:105129. doi: 10.1016/j.fitote.2022.105129
- Grimblat, N., Zanardi, M. M., and Sarotti, A. M. (2015). Beyond DP4: an improved probability for the stereochemical assignment of isomeric compounds using quantum chemical calculations of NMR shifts. *J. Organomet. Chem.* 80, 12526–12534. doi: 10.1021/acs.joc.5b02396
- Halgren, T. A. (1999). MMFF VI. MMFF94s option for energy minimization studies. *J. Comput. Chem.* 20, 720–729. doi: 10.1002/(SICI)1096-987X(199905)20:7<720::AID-JCC7>3.0.CO;2-X
- Kahlert, L., Bassiony, E. F., Cox, R. J., and Skellam, E. J. (2020). Diels-alder reactions during the biosynthesis of sorbicillinoids. *Angew. Chem. Int. Ed.* 59, 5816–5822. doi: 10.1002/anie.201915486
- Kumar, P., Wallis, M., Zhou, X., Li, F., Holland, D. C., Reddell, P., et al. (2024). Triplinones A-H: anti-inflammatory arylalkenyl α,β -unsaturated- δ -lactones isolated from the leaves of Australian rainforest plant *Cryptocarya triplinervis* (Lauraceae). *J. Nat. Prod.* 87, 1817–1825. doi: 10.1021/acs.jnatprod.4c00454
- Li, J. T., Yin, B. L., Liu, Y., Wang, L. Q., and Chen, Y. G. (2009). Mono-aromatic constituents of *Dendrobium longicornu*. *Chem. Nat. Compd.* 45, 234–236. doi: 10.1007/s10600-009-9293-2
- Peng, X. P., Li, G., Wang, L. M., Wang, Q., Wang, C., Ji, L. X., et al. (2022). Structurally various sorbicillinoids from an endophytic fungus *Acremonium citrinum* SS-g13. *Front. Microbiol.* 13:800626. doi: 10.3389/fmicb.2022.800626
- Rehman, S. U., Yang, L. J., Zhang, Y. H., Wu, J. S., Shi, T., Haider, W., et al. (2020). Sorbicillinoid derivatives from sponge-derived fungus *Trichoderma reesei* (HN-2016-018). *Front. Microbiol.* 11:1334. doi: 10.3389/fmicb.2020.01334
- Sib, A., and Gulder, T. A. M. (2017). Stereoselective total synthesis of bisorbicillinoid natural products by enzymatic oxidative dearomatization/dimerization. *Angew. Chem. Int. Ed.* 56, 12888–12891. doi: 10.1002/anie.201705976
- Wang, Y. J., Chen, X., Yin, Y., Zhou, W., Zhou, P. F., Zeng, L. G., et al. (2024). Hedscondines A-C, three undescribed indole alkaloids from *Hedyotis scandens* with their anti-MRSA activity. *Phytochemistry* 219:113988. doi: 10.1016/j.phytochem.2024.113988
- Wang, Y., Li, X. M., Yang, S. Q., Zhang, F. Z., Wang, B. G., Li, H. L., et al. (2022). Sesquiterpene and sorbicillinoid glycosides from the endophytic fungus *Trichoderma longibrachiatum* EN-586 derived from the marine red alga *Laurencia obtusa*. *Mar. Drugs* 20:177. doi: 10.3390/md20030177
- Wang, F., Zhang, M., Yuan, M., Xia, Z., Yang, F., Zhang, S., et al. (2023). A novel sorbicillinoid compound as a potent anti-inflammation agent through inducing NLRP3 protein degradation. *Br. J. Pharmacol.* 180, 1930–1948. doi: 10.1111/bph.16058
- Willoughby, P. H., Jansma, M. J., and Hoye, T. R. (2014). A guide to small-molecule structure assignment through computation of (^1H and ^{13}C) NMR chemical shifts. *Nat. Protoc.* 9, 643–660. doi: 10.1038/nprot.2014.042
- Xie, C. L., Zhang, D., Lin, T., He, Z. H., Yan, Q. X., Cai, Q., et al. (2021). Antiproliferative sorbicillinoids from the deep-sea-derived *Penicillium allii-sativi*. *Front. Microbiol.* 11:636948. doi: 10.3389/fmicb.2020.636948
- Yin, G. P., Gong, M., Li, Y. J., Zhang, X., Zhu, J. J., and Hu, C. H. (2021a). 14-membered resorcylic acid lactone derivatives with their anti-inflammatory from the fungus *Aspergillus* sp. ZJ-65. *Fitoterapia* 151:104884. doi: 10.1016/j.fitote.2021.104884
- Yin, G. P., Gong, M., Xue, G. M., Gong, T., Cao, X., Wang, W., et al. (2021b). Penispidins A-C, aromatic sesquiterpenoids from *Penicillium virgatum* and their inhibitory effects on hepatic lipid accumulation. *J. Nat. Prod.* 84, 2623–2629. doi: 10.1021/acs.jnatprod.1c00185
- Yin, G. P., Li, Y. J., Zhang, L., Zeng, L. G., Liu, X. M., and Hu, C. H. (2024). Citrinsorbicillin a, a novel homotrimeric sorbicillinoid isolated by LC-MS-guided with cytotoxic activity from the fungus *Trichoderma citrinoviride* HT-9. *Chin. Chem. Lett.* 35:109035. doi: 10.1016/j.ccl.2023.109035

- Ying, Y., Lei, P., Xu, Y., Lin, Y., Yang, N., Han, Y., et al. (2024). Secondary metabolites from *Penicillium* sp. HS-11, a fungal endophyte of *Huperzia serrata*. *Fitoterapia* 175:105943. doi: 10.1016/j.fitote.2024.105943
- Yu, X., Müller, W. E. G., Frank, M., Gao, Y., Guo, Z., Zou, K., et al. (2024). Caryophyllene-type sesquiterpenes from the endophytic fungus *Pestalotiopsis lespedezae* through an OSMAC approach. *Front. Microbiol.* 14:1248896. doi: 10.3389/fmicb.2023.1248896
- Zhang, P., Deng, Y., Lin, X., Chen, B., Li, J., Liu, H., et al. (2019). Anti-inflammatory mono- and dimeric sorbicillinoids from the marine-derived fungus *Trichoderma reesei* 4670. *J. Nat. Prod.* 82, 947–957. doi: 10.1021/acs.jnatprod.8b01029
- Zhang, Y., Zhang, J., Du, Q., Wu, X. M., Chen, Y., and Tan, R. X. (2024a). Citrisorbicillinol, an undescribed hybrid sorbicillinoid with osteogenic activity from *Penicillium citrinum* ZY-2. *Fitoterapia* 173:105836. doi: 10.1016/j.fitote.2024.105836
- Zhang, Y., Zhang, Y., Li, G., Dong, K., Wang, J., Xiao, S., et al. (2024b). Anti-inflammatory monomeric sorbicillinoids from the marine-derived fungus *Trichoderma* sp. G13. *Fitoterapia* 175:105963. doi: 10.1016/j.fitote.2024.105963
- Zhang, X. H., Zhang, D. J., Liu, J. L., Pan, H. Y., Qin, J. C., and Zhang, Y. H. (2018). Antifungal effects of volatile organic compounds from the endophytic fungus *Cryptosporiopsis ericae* cc-HG-7 isolated from *Coptis chinensis* Franch. *Biocontrol Sci. Tech.* 28, 496–508. doi: 10.1080/09583157.2018.1460744
- Zhao, Y., Liu, J. P., Lu, D., Li, P. Y., and Zhang, L. X. (2010). A new antioxidant xanthone from the pericarp of *Garcinia mangostana* Linn. *Nat. Prod. Res.* 24, 1664–1670. doi: 10.1080/14786419.2010.499539
- Zhao, D. L., Wang, H. S., Gao, L. W., and Zhang, P. (2022). Tennesenoid A, an unprecedented steroid-sorbicillinoid adduct from the marine-derived endophyte of *Aspergillus* sp. strain 1022LEF. *Front. Mar. Sci.* 9:923128. doi: 10.3389/fmars.2022.923128
- Zou, M., Wang, R., Yin, Q., and Liu, L. (2021). Bioassay-guided isolation and identification of anti-alzheimer's active compounds from *Spiranthes sinensis* (Pers.) Ames. *Med. Chem. Res.* 30, 1849–1855. doi: 10.1007/s00044-021-02777-8